MATERIALS SCIENCE

Looping-in complexation and ion partitioning in nonstoichiometric polyelectrolyte mixtures

Sean Friedowitz[1,2†], Junzhe Lou[1,3†], Kayla Patricia Barker[3], Karis Will[3‡], Yan Xia[3]*, Jian Qin[2]*

A wide variety of intracellular membraneless compartments are formed via liquid-liquid phase separation of charged proteins and nucleic acids. Understanding the stability of these compartments, while accounting for the compositional heterogeneity intrinsic to cellular environments, poses a daunting challenge. We combined experimental and theoretical efforts to study the effects of nonstoichiometric mixing on coacervation behavior and accurately measured the concentrations of polyelectrolytes and small ions in the coacervate and supernatant phases. For synthetic polyacrylamides and polypeptides/DNA, with unequal mixing stoichiometry, we report a general "looping-in" phenomenon found around physiological salt concentrations, where the polymer concentrations in the coacervate initially increase with salt addition before subsequently decreasing. This looping-in behavior is captured by a molecular model that considers reversible ion binding and electrostatic interactions. Further analysis in the low-salt regime shows that the looping-in phenomenon originates from the translational entropy of counterions that are needed to neutralize nonstoichiometric coacervates.

INTRODUCTION

Solutions of polycations and polyanions under proper conditions may exhibit a demixing transition, resulting in the coexistence of a polymer-rich phase known as polyelectrolyte complex coacervate (PEC) and a dilute supernatant nearly devoid of polymers (*1*). PECs may appear as solid-like precipitates or as viscoelastic fluids, commonly referred to as coacervates (*2*). Since the discovery of coacervation from biopolymers (*1*), PECs have garnered much attention for use as protein and drug encapsulants (*3*), gene delivery vehicles (*4*, *5*), surface coatings (*6*), and adhesives (*7*). Recent interest in PECs is spurred by the findings that coacervation is the mechanism underlying the formation of membraneless liquid organelles in cells, including P-bodies (*8*), stress granules (*9*), and germ granules (*10*). In these contexts, coacervation is often referred to as liquid-liquid phase separation (LLPS) and is thought to play a critical role in the spatial and temporal organization of biochemical reactions (*11*, *12*) and in gene regulation (*8*, *13*). For example, P-bodies and stress granules function as storage sites for mRNAs and cooperatively regulate mRNA translation and degradation (*8*, *14*). Stress granules are formed in response to exogenous stresses and turn off translation by sequestering untranslated mRNAs and translation initiation factors (*14*, *15*).

A distinct feature of LLPS in biological settings is the heterogeneity in sequence, conformation, and composition of the participating polymers (i.e., proteins and nucleic acids) (*16*–*18*). Despite increasing efforts, it remains unclear whether the thermodynamics of LLPS is governed by simple rules, especially in solutions with heterogeneous compositions. Several in vitro studies using purified proteins and polynucleotides have highlighted the importance of the mixing ratio between oppositely charged polyelectrolytes (PEs) in dictating coacervate stability. Livolant and coworkers found that DNA can be condensed and resolubilized by continuously increasing concentration of multivalent cationic partners (*19*, *20*). More recently, Gladfelter and coworkers showed that, under physiological conditions, phase separation between mRNA and the Whi3 protein would not occur at highly asymmetric mixing ratios (*21*). Brangwynne and coworkers studied the stability of PECs against salt addition by fixing the concentration of rRNA and varying that of NPM1 protein (*22*). Their phase diagram (*22*) implies a salting-out behavior at highly unequal RNA/protein ratios, where adding salt causes an initially homogeneous solution to phase separate. A fundamental understanding of the role played by the mixing ratio and a detailed characterization of the coexisting phases is, however, missing.

Tackling this issue using synthetic PEs with well-defined stoichiometry is desirable in that the uncertainty in biological PECs is eliminated. Past research using synthetic polymers has identified several molecular parameters that strongly influence coacervation behavior, including polymer molecular weight (*23*, *24*), patterning of charge groups on the polymer chains (*25*), and the local environment around charges (*26*). However, these studies investigated mixtures of polyanions and polycations at equal charge stoichiometry, which is an extremely unlikely scenario in biological PECs. Moreover, most of these studies focused on the critical salt concentrations that are generally much higher than physiological conditions, making them less relevant for understanding biological PECs.

A challenge of studying PECs formed from nonstoichiometric solutions is determining the concentrations of all ionic species within each phase. The partitioning of PEs between coexisting phases is critical for understanding the thermodynamics of coacervation. Previous studies could not differentiate the concentrations of polycations and polyanions and thus treated them as identical (*23*, *24*, *26*), which is, at best, a poor assumption for nonstoichiometric mixtures. Therefore, the compositions and phase behavior of PECs with unequal PE stoichiometry remain largely unknown.

In parallel, much theoretical progress has been made to model the coacervation process (*27*–*29*). The early work by Overbeek and Voorn (*30*) embedded the Debye-Hückel theory to the standard expression for the solution free energy and described coacervation

[1]Department of Materials Science and Engineering, Stanford University, Stanford, CA 94305, USA. [2]Department of Chemical Engineering, Stanford University, Stanford, CA 94305, USA. [3]Department of Chemistry, Stanford University, Stanford, CA 94305, USA.
*Corresponding author. Email: yanx@stanford.edu (Y.X.); jianq@stanford.edu (J.Q.)
†These authors contributed equally to this work.
‡Present address: Harvard University, Massachusetts General Hospital, Boston, MA 02114, USA.

as a result of the competition between mixing entropy and electrostatic correlations. Since then, a wealth of molecular details, including chain connectivity (*31*, *32*), short-range ion binding (*33*–*38*), dipolar interactions (*39*), and charge patterning and sequence (*25*, *40*), have been investigated. Most of these studies have followed the experimental efforts and focused on stochiometrically symmetric solutions. One notable exception is a recent study that examined coacervation behavior following a variety of asymmetric mixing protocols (*41*).

Here, we report joint experimental and theoretical efforts to examine the role of mixing ratio in polyelectrolyte complex coacervation. We prepared PECs using PEs with identical backbones and oppositely charged side groups and quantified the concentrations of all ionic species in both coacervate and supernatant phases using fluorescent labeling of the PEs and inductively coupled plasma mass spectroscopy (ICP-MS). These measurements allowed us to construct full phase diagrams for each mixing ratio, which revealed a hitherto unexplored "looping-in" phenomenon in the low-salt regime for asymmetric (i.e., nonstoichiometric) mixing ratios. The polymer concentrations in the coacervate were found to initially increase and then decrease upon salt addition, in contrast to the well-known "salting-in" behavior in stoichiometric mixtures, where the polymer concentration decreases monotonically with increasing salt concentration. We further confirmed the generality of our findings by observing analogous phenomena in PECs prepared from biomacromolecules, including polypeptides and polynucleotides.

To understand the origin of this looping-in behavior, we analyzed the experimental results using a model that combines the short-range ion binding equilibrium and long-range electrostatic interactions (*37*). In our recent work on stoichiometric solutions (*26*), this model simultaneously captured the effects of polymer molecular weight and local hydrophilicity on PEC formation. Here, this model also captures the variation of phase diagrams with mixing ratio and reveals the same looping-in phenomenon at low salt concentrations. Examining the phase coexistence condition in the low-salt regime showed that the looping-in behavior is closely tied to the mixing entropy of counterions in the coacervate and the strength of electrostatic correlations. We find that the abundance of neutralizing counterions influences the partitioning of added salts between the supernatant and coacervate, and consequently, the variation of the polymer concentration in the coacervate, although exactly how the polymer concentration changes, depends on the treatment of electrostatic correlations.

RESULTS

Looping-in complexation in nonstoichiometric mixtures

Previous experimental PEC phase diagrams have either quantified a single PE concentration (*23*, *26*) or the total PE concentration (*2*, *24*) in the supernatant and coacervate phases. These measurements are insufficient when oppositely charged PEs are mixed at unequal ratios, as the stoichiometry of the coexisting phases is not known a priori. We have synthesized charged polyacrylamides with pendent ammonium or sulfate groups at identical chain lengths (degree of polymerization, $N = 50$) and charge density from the same narrow-disperse polymer precursor made by controlled radical polymerization, following our recently reported method (*26*). To independently quantify the concentrations of polycations and polyanions in PECs, we developed a strategy to individually label the polyanions and polycations using two different fluorescent dyes with nearly baseline separation in their ultraviolet-visible (UV-vis) absorption spectra (Fig. 1A). Polycations were labeled with rhodamine B (RB; $\lambda_{max} = 566$ nm) at a fraction of approximately 1 per 10 polymer chains and the polyanions with sulfo-cyanine5 (Cy5; $\lambda_{max} = 649$ nm) at a fraction of approximately 1 per 87 polymer chains. The average degree of labeling on PEs was determined by the ^{1}H nuclear magnetic resonance (NMR) or UV-vis spectroscopy of labeled polymers (*26*).

These PEs were mixed at a total polymer concentration of 100 mM and with varying stoichiometric ratios between oppositely charged chains (see Materials and Methods for details on mixing protocols). The fluorescent dyes attached to the polymers allowed for direct visualization of the partitioning of oppositely charged PEs upon phase separation. The blue tinted color was from the Cy5-labeled polyanions, and the pink color was from the RB-labeled polycations. When the polyacrylamide PEs were mixed at a 1:1 ratio of polyanions to polycations (A:C), and NaCl are added, whose concentrations range from 0 to 1.2 M, the color intensity of the supernatant phase clearly increased, indicating a higher PE concentration in the supernatant phase (Fig. 1B). However, when mixed at unequal stoichiometry at the same total polymer concentration (100 mM), the color intensity of the supernatant without any added salt was stronger than that with relatively low concentration of salt (0.1 to 0.2 M). This phenomenon is in stark contrast to common observations when PEs are mixed at equal stoichiometry: Increasing salt concentration generally destabilizes the coacervate phase and results in a greater concentration of polymers in the supernatant (*23*, *24*, *26*). This regime of salt concentrations is relevant to the physiological salt concentrations found in both the cytosol and extracellular matrices of cells (about 0.15 M).

With the dual fluorescent labeling and ICP-MS techniques, we were able to individually determine the concentrations of all species in the supernatant and coacervate phases. This allowed us to generate phase diagrams in terms of the total ion and polymer concentrations within each phase (Fig. 2). In these plots, the *y* axis represents the total concentration of all salt ions, including the counterions of the PEs, and the *x* axis represents the total concentration of both polymers (in terms of repeat units). To guide the eye, data points representing the coexisting coacervate and supernatant phases for the 3:1 A:C mixing ratio are connected. These lines should not be interpreted as tie lines because cations and anions are partitioned differently between the two phases. The full coexistence condition is a three-dimensional surface [see (*41*), Fig. 2, and fig. S12], and the quantitative partition coefficients for individual polymers and ions are shown in Fig. 3.

When polyanions and polycations were mixed at 1:1 molar ratio, the phase diagram showed the typical open-dome shape, where the width of the two-phase region beneath the dome decreased with increasing added salt (Fig. 2). Binodal phase diagrams for PEs mixed at an unequal stoichiometry showed decreased overall coacervate stability. The two-phase regions became narrower with increasing mixing asymmetry. The maximum ion concentrations, which are observed from the points with the greatest amount of added salt on each binodal phase diagram, also decreased slightly for nonstoichiometric mixing.

For asymmetrically mixed solutions, a notably different trend in phase diagram shape was observed at low salt concentrations. In these cases, the total polymer concentration in the coacervate phase initially increased for added salt concentrations between 0.05 and

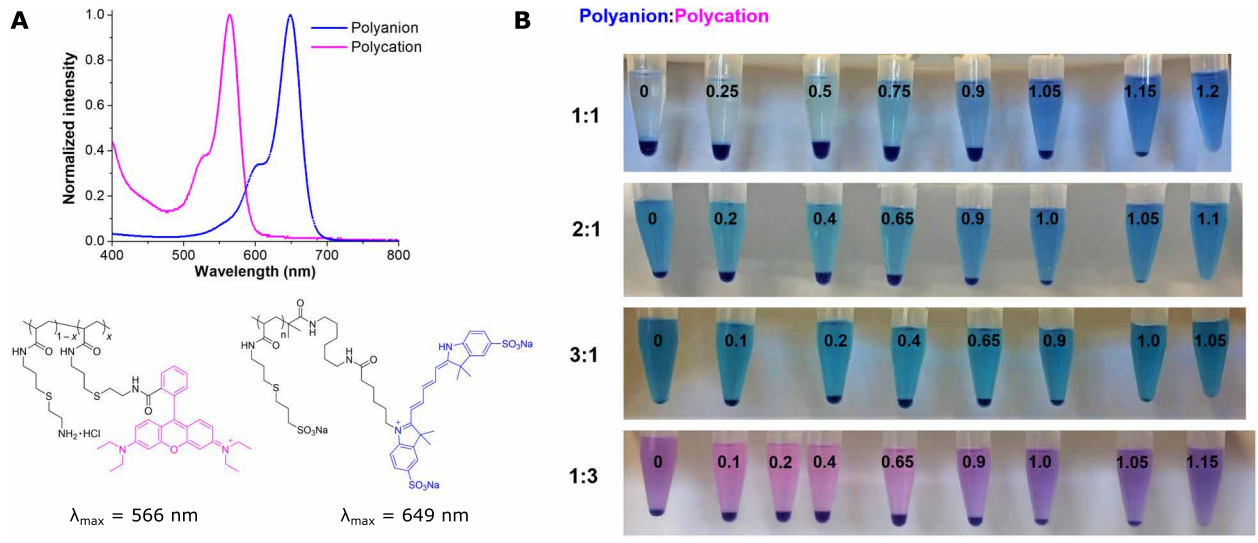

Fig. 1. Dual fluorescent labeling of polyacrylamides. (**A**) Chemical structures of RB-labeled polycations and Cy5-labeled polyanions, and the UV absorption spectra of these PEs. (**B**) Photograph of phase separation upon mixing of oppositely charged PEs at different mixing ratios. Molar concentrations of added NaCl are labeled on top of each sample tube. Photo credit: Junzhe Lou, Stanford University.

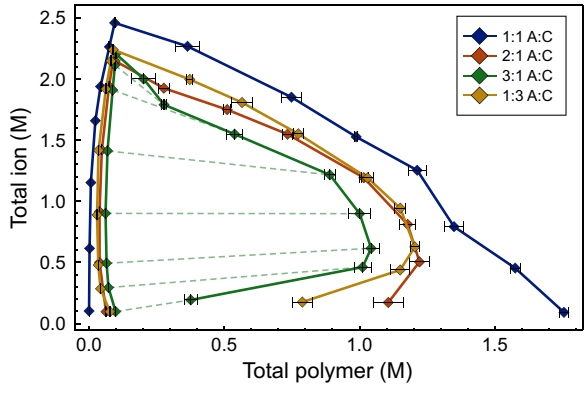

Fig. 2. Nonstoichiometric phase diagrams for polyacrylamides. Experimental phase diagrams for synthetic polyacrylamide PEs with different mixing ratios and a total polymer concentration of 0.1 M.

0.25 M, before subsequently decreasing. This observation resulted in a looping-in shape in the phase diagram. The looping-in shape was observed when either polyanions or polycations were in excess, which became more pronounced with greater extents of mixing asymmetry (i.e., 3:1 as compared to 2:1 ratios). When the concentration of added salt was above 1.0 M, asymmetric PECs became homogeneous solutions, and phase separation ceased to occur, analogous to the samples prepared at a 1:1 mixing ratio.

Typically, adding salt to a coacervate-forming system is expected to destabilize the PECs until an upper maximum salt concentration is reached, and a homogeneous solution reappears (i.e., salting-in). This trend is exactly what we observed in the case of a 1:1 mixing ratio. However, the looping-in shape of the phase diagram for asymmetric mixing represents a salting-out phenomenon, where an initially homogeneous solution spontaneously demixes once enough salt is added so that the solution falls within the two-phase region. The appearance of a salting-out phenomenon has been previously described theoretically for solutions consisting of a single PE species (*42*). Given that equal mixing stoichiometry is an extreme rarity in nature, this observed salting-out behavior under physiologically relevant salt concentrations hints at a means of controlling PEC formation through perturbations in solution conditions.

Partitioning of PEs and small ions

A difficulty in the study of PECs is the quantification of the concentrations of all ionic species within the coacervate and supernatant phases. Our dual fluorescent labeling of PEs allowed us to accurately measure their concentrations and partitioning coefficients between the coexisting phases (see Materials and Methods and Supplementary Text for details on the quantification methods).

When polyanions and polycations were mixed at equal molarity, their concentrations in the coacervate phase were nearly equal. In contrast, when mixed at unequal ratios, the concentration asymmetry between polyanions and polycations in the formed coacervates was reduced compared to the stoichiometry of their initial loading. These trends can be quantified by introducing the overcharging of the coacervate, defined as

$$\%\ \text{Overcharging} = 100 \times ([A]/[C] - 1) \quad (1)$$

where [A] and [C] denote the concentrations of the polyanions and polycations in the coacervate. Figure 3A shows that, for the asymmetrically mixed solutions, the observed overcharging is significantly less than the expected values based on the initial mixing ratios (shown as dashed lines in Fig. 3A). This reduced overcharging was present for solutions with excess polyanion (i.e., 2:1 and 3:1 A:C samples) or polycation (i.e., 1:3 A:C sample). We note that, for the overcharged coacervate to be electroneutral, an excess of oppositely charged counterions must be present. The implication of these excess counterions in the coacervate is explored further in our theoretical analysis.

ICP-MS has been widely used to detect elemental ions in solutions with part per billion (ppb) level sensitivity and tolerance of a background of other ions and molecules. The ICP-MS measurements

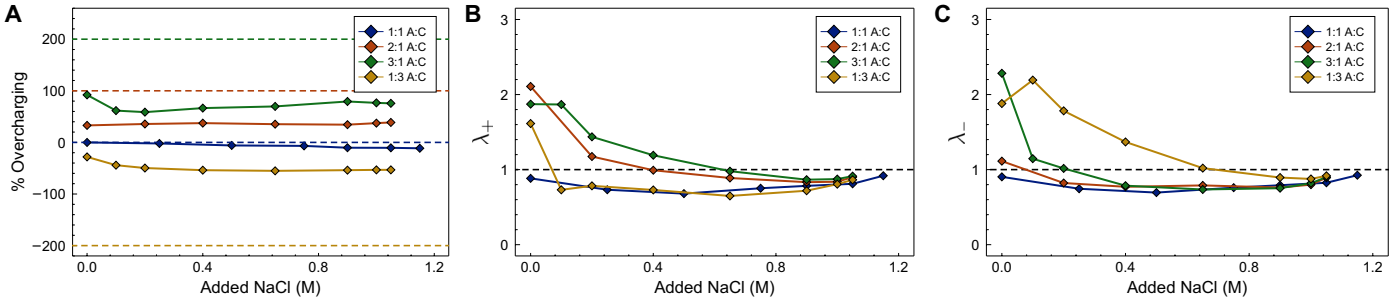

Fig. 3. Polymer and ion partitioning of polyacrylamide coacervates. (**A**) Overcharging of the coacervate versus the total added ion concentration for different mixing ratios. Dashed lines represent the ideal overcharging percentage based on the initial solution stoichiometry. (**B** and **C**) Ion partition coefficients for (B) Na^+ and (C) Cl^- ions as a function of added salt in the initial solution. The added NaCl concentration is the amount of salt added to the initial solutions and does not represent the total ion concentration along the phase diagrams, which includes the counterions of the PEs.

allowed us to directly measure the partition coefficients of small ions, defined by

$$\lambda_+ = [+]_2/[+]_1 \quad (2)$$

$$\lambda_- = [-]_2/[-]_1 \quad (3)$$

where [+] and [−] represent the concentrations of the cations and anions, and the subscripts 1 and 2 denote the concentrations in the supernatant and coacervate phases. A value of $\lambda_\pm > 1$ indicates preferential partitioning of the ions to the coacervate phase, and $\lambda_\pm < 1$ indicates the opposite, i.e., ions prefer to enter the supernatant.

With equimolar polymer mixing ratios, we found that both λ_+ and λ_- are less than unity for all added salt concentrations, indicating negative tie-line slopes and preferential ion partitioning to the supernatant (Fig. 3, B and C). This observation is consistent with previous experimental work and theoretical predictions (*24*). For all the asymmetrical mixtures, both λ_+ and λ_- are greater than unity at low salt concentrations and fall below unity at higher salt concentrations. This change in slope occurs at approximately the same salt concentration where the looping-in behavior ends and the coacervate polymer concentrations begin to decrease, suggesting that the variation in the coacervate polymer concentration is related to how ions partition between the coexisting phases.

Asymmetric mixing of polypeptide and DNA solutions

To examine the generality of the observed looping-in phenomenon for asymmetric mixtures, we studied PEs with different backbone structures and charge moieties that have closer biological relevance. We first examined PECs between charged polypeptides, poly(D,L-glutamic acid) (PGA) and poly(L-lysine) (PLL). Both polypeptides were synthesized via *N*-carboxyanhydride (NCA) polymerization initiated by hexamethyldisilazane with controlled degree of polymerization (N = 50) and low polydispersity. To accurately quantify concentrations of these polymers, PGA was sparsely labeled with Cy5 at an approximate fraction of 1 per 295 polymer chains and PLL with fluorescein isothiocyanate (FITC) at a fraction of approximately 1 per 32 polymer chains. These dyes have distinct absorption peaks in UV-vis spectra to allow independent quantification of each polypeptide in the two phases (fig. S10).

Phase diagrams for mixtures of PGA and PLL solutions are plotted in Fig. 4A, where the y axis is the added concentration of NaCl and the x axis is the total polymer concentration. In this case, the individual ion concentrations were not determined by ICP-MS, so the diagrams indicate only the concentration of salt that was added to the solution. When PGA and PLL were mixed at 1:1 molar ratio with an overall concentration of 100 mM, phase separation occurred below the upper maximum salt concentration of 0.70 M NaCl. The phase diagram for symmetric solutions showed a typical open coacervation dome. When PGA and PLL were mixed at a 3:1 ratio, we again observed the looping-in phenomenon at low NaCl concentrations between 0 and 0.25 M.

Using the charged polypeptides, we also visualized the dynamics of coacervate formation and dissolution as salt was continuously added to the system. When PGA and PLL were mixed at 9:1 ratio with an overall concentration of 100 mM, a clear solution was obtained without added salt (Fig. 4B). The addition of a small amount of NaCl (0.1 M in the mixture) resulted in phase separation, indicating the suspected salting-out behavior at low salt concentrations (movie S1). The volume of the added NaCl solution was small and had negligible effect on the polymer concentrations in the mixture. When more NaCl was added, the salting-in behavior was ultimately observed, and the mixture turned clear again (Fig. 4B).

Next, we studied mixtures of PLL and single-stranded DNA (ssDNA), a system that closely mimics the general components of many liquid organelles [i.e., intrinsically disordered proteins and polynucleotides; (*17*)]. Because of the limited DNA quantity, we use turbidity measurements to quantify phase separation. Measuring turbidity is a common method to study PECs (*43*, *44*), although it does not provide precise measurement of the extent of phase separation. We measured the turbidity upon mixing the two polymers at various stoichiometric ratios and an overall concentration of 8 mM (Fig. 4C). When PLL and ssDNA were mixed at 1:1 molar ratio, the turbidity was high at low salt concentrations (<0.6 M) and decreased rapidly at higher salt concentrations (>0.6 M). In contrast, when the mixing ratios were unequal, with PLL:ssDNA = 3:1 or 7:1, the turbidity was minimal without added salt but markedly increased when 0.1 M of NaCl was added. Further increasing the salt concentration resulted in a decrease in turbidity and ultimately the reappearance of a homogeneous solution.

Direct imaging of the coacervate droplets by confocal microscopy confirmed the trend from turbidity measurements (Fig. 4D). At a 7:1 mixing ratio without added salt, very few coacervate droplets (appearing green due to the FITC dyes labeled on PLL) were observed upon mixing. When 0.2 M NaCl was added to the mixture, the number and size of droplets increased significantly. When the

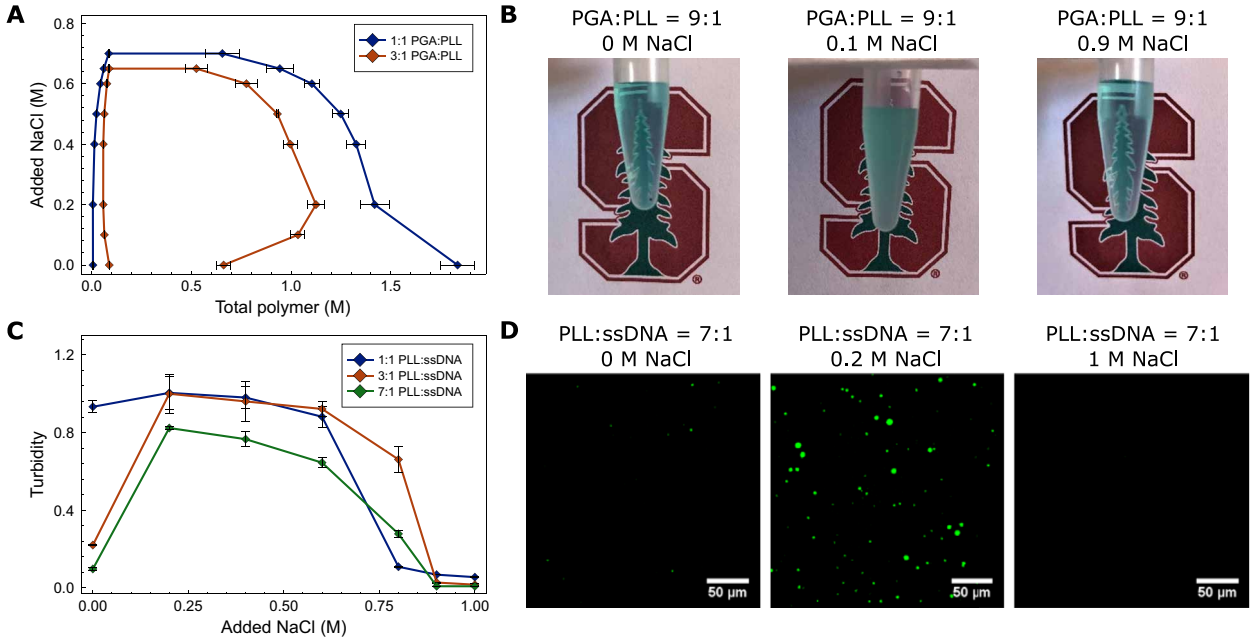

Fig. 4. Nonstoichiometric coacervation of polypeptides and DNA. (**A**) Experimental phase diagrams for PGA and PLL with different mixing ratios at a total polymer concentration of 100 mM. (**B**) Photograph of PGA and PLL at 9:1 mixing ratios containing 0, 0.1, and 0.9 M of NaCl, showing salting-out at low salt concentrations and salting-in at high salt concentrations. Photo credit: Junzhe Lou, Stanford University. (**C**) Turbidity of PLL and ssDNA with different mixing ratios at an overall concentration of 8 mM. (**D**) Confocal images of coacervates formed between PLL and ssDNA at a 7:1 ratio.

added NaCl concentration exceeded 1.0 M, the coacervate droplets disappeared. These images are consistent with the looping-in behavior that we observed with the other polymer mixtures. Notably, the added salt concentrations where looping-in occurs were again between 0 and 0.2 M, which are close to the salt concentrations under physiological conditions in the human body.

Overall, the similar coacervation phase behavior observed for different PEs, charged polyacrylamides, polypeptides, and DNA at asymmetric mixing ratios suggests that this looping-in behavior is a general phenomenon regardless of the specific PE chemistry.

Theoretical predictions of asymmetric phase diagrams

The phase diagrams and the looping-in behavior for polyacrylamide PEs are captured by the theoretical model that we developed previously (*26*, *35*, *37*, *38*). The model expresses the solution free energy as a sum of the mixing entropy of all species, dispersion interactions, and electrostatic correlations described by the random phase approximation (RPA) (*32*, *37*). The model optimizes the polymer charge density by minimizing the solution free energy over the degrees of three reversible ion binding "reactions": anion localization near the polycations, cation localization near polyanions, and the formation of interchain "ion-pairs" or cross-links between oppositely charged polymers, i.e.,

$$(\mathrm{A}) + (+) \overset{\Delta G^{\mathrm{eff}}_{\mathrm{A+}}}{\rightleftharpoons} (\mathrm{A}+) \tag{4}$$

$$(\mathrm{C}) + (-) \overset{\Delta G^{\mathrm{eff}}_{\mathrm{C-}}}{\rightleftharpoons} (\mathrm{C}-) \tag{5}$$

$$(\mathrm{A}) + (\mathrm{C}) \overset{\Delta G^{\mathrm{eff}}_{\mathrm{AC}}}{\rightleftharpoons} (\mathrm{AC}) \tag{6}$$

Here, $\Delta G^{\mathrm{eff}}_{\mathrm{A+}}$, $\Delta G^{\mathrm{eff}}_{\mathrm{C-}}$, and $\Delta G^{\mathrm{eff}}_{\mathrm{AC}}$ are the effective reaction free energies, which are each composed of a short-range contribution (denoted $\Delta G_{\mathrm{A+}}$, $\Delta G_{\mathrm{C-}}$, and ΔG_{AC}, respectively) and a long-range contribution derived from the electrostatic correlation free energy. Full algebraic details of our model are provided in Supplementary Text.

The coexistence diagrams are constructed by sweeping the concentration of added salt for a fixed mixing ratio between the polymers and balancing the chemical potential of each component between the phases (see Supplementary Text). To quantitatively capture the experimental trends, the binding free energies, $\Delta G_{\mathrm{A+}}$, $\Delta G_{\mathrm{C-}}$, and ΔG_{AC}, and the Flory-Huggins χ parameter between the polymer and solvent, χ_{PW} (the polycations and polyanions have identical backbones and thus χ parameters), are fit against the phase diagram for the 1:1 A:C mixture. These parameters are then used to predict the phase diagrams for the 2:1 and 3:1 A:C cases. Further details on our phase diagram construction and fitting procedures are provided in Materials and Methods.

The theoretical phase diagrams for 1:1, 2:1, and 3:1 A:C mixtures are compared with the experimental data in Fig. 5, where the *y* axis is the total ion concentration and the *x* axis is the individual polyanion or polycation concentrations for each phase. The partition coefficients for cations and anions are individually shown in Fig. 6. The result for the 1:3 mixing ratio is omitted because the prediction is identical to that for the 3:1 mixture.

For the 1:1 mixture, the agreement between the experimental data and theoretical prediction on the maximum salt concentration and the coexistence window width is similar to our previous work (*26*). Further, our theory predicts an ion-enriched supernatant (negative tie-lines) for both cations and anions (Fig. 6, B and C), in

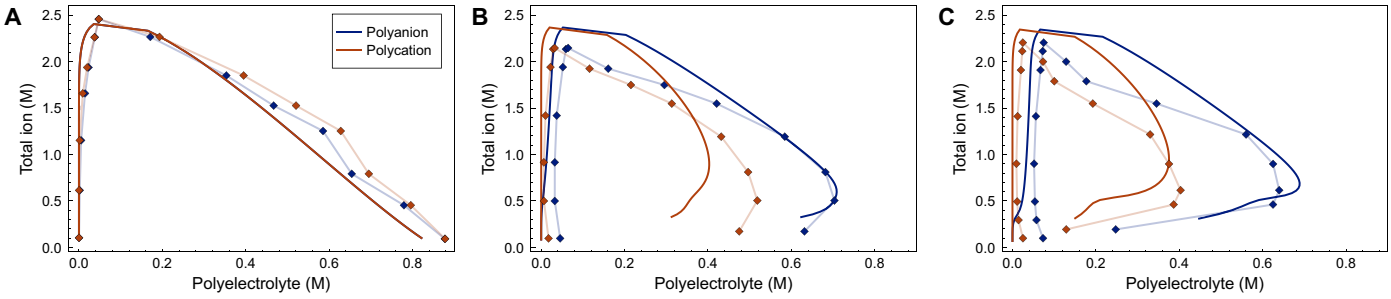

Fig. 5. Theoretical predictions of phase diagrams prepared for mixtures of synthetic polyacrylamide PEs. Results for mixing ratios of (**A**) 1:1, (**B**) 2:1, and (**C**) 3:1 polyanion to polycation. Solid lines are theoretical predictions, and diamond markers are experimental data points. Fitting parameters: $\chi_{PW} = 0.5$, $\Delta G_{A+} = \Delta G_{C-} = -1.0$, and $\Delta G_{AC} = -1.55$ (see Materials and Methods).

agreement with the experimental data and previous reports (*24*, *44*). We note that, with different binding free energies, the sign of the tie-line slopes may become positive, which highlights the importance of short-range interactions in quantitative predictions of coacervation phase behavior (*35*, *38*).

By using identical model parameters as for the symmetric case, our theoretical predictions capture the variation of both the polyanion and polycation concentrations for the asymmetric mixing ratios, 2:1 and 3:1. In particular, the range of salt concentrations (≤ 0.5 M) over which the looping-in behavior is observed is nearly quantitatively captured. The narrowing of the two-phase window and the suppression of the maximum salt concentration with increased concentration asymmetry are also consistent with the experimental trends.

On the other hand, the predicted polymer concentrations in the supernatant are evidently lower than the experimental values. This is especially true in the low-salt regime, where the theory predicts a nearly polymer-depleted supernatant. Consequently, the ratio of polymer concentrations in the coacervate is similar to the initial solution, and the predicted overcharging is much higher than the experimental observation (Fig. 6A). We attribute this discrepancy to the treatment of the chains as flexible coils in the RPA expression for the electrostatic free energy, which is known to overestimate electrostatic correlations and significantly underestimate the supernatant concentrations (*45*, *46*). The small variations along the coacervate branch at low salt concentrations in Fig. 5 (B and C) is a result of this shift in polymer partitioning.

Both theoretical and experimental results show that the excess counterions (the cations) are enriched in the coacervate at low salt concentrations (Fig. 6B), which is required to neutralize the surplus charge from the polyanions in the coacervate. Because the predicted overcharging for asymmetric mixtures is higher than the experimental values (Fig. 6A), the predicted partition coefficient λ_+ is also higher. Conversely, our theory predicts that the anions preferentially partition to the supernatant at all salt concentrations, resulting in a partition coefficient λ_- less than unity (Fig. 6C). This apparently contrasts with the experimental results: In the low-salt regime, the anions are also enriched in the coacervate. Two factors may be responsible for this discrepancy. First, the RPA-based treatment of electrostatics significantly underestimates the supernatant polymer concentrations, which affects how anions are partitioned. Second, for strongly asymmetric mixtures at low salt concentrations, the coacervate sample volumes are extremely small (Fig. 1B, third row), which increases the uncertainty in the measured salt concentrations.

The different partitioning behavior for the cations and anions can be reconciled by considering the electroneutrality constraint. In an asymmetric PEC with excess polyanions, the cations are composed of two groups, charge-neutralizing counterions and any excess cations due to salt addition. The counterion concentration is fixed by the extent of overcharging of the coacervate. The excess cations are found to be depleted from the coacervate at all salt concentrations, and the corresponding partition coefficient is identical to that of the anions in the low-salt regime (fig. S11). The implication of this ion partitioning behavior on the looping-in phenomenon is discussed in the next section.

Theoretical predictions on the width of the two-phase window and the response to salt addition are sensitive to the conformational properties of polymers. As demonstrated in fig. S12, we find that chains with flexible, coil-like conformations result in the low-salt looping-in behavior for asymmetric mixtures, yet stiffer rod-like chains do not, resembling the results of a previous study (*41*). This suggests that sufficiently strong electrostatic correlations, stemming from the flexibility of coil-like chains, is needed to produce the looping-in behavior, which contributes to the excess chemical potential of ions, as we show explicitly in the next section (Eq. 9). The strength of our theory is that it nearly quantitatively captures the behavior for both symmetric and asymmetric mixtures. However, as discussed below, a generic mechanism is at play, suggesting that the looping-in behavior in nonstoichiometric solutions is universal, and not strictly dependent on the details of our model.

DISCUSSION

Origin of looping-in coacervation at low salt concentrations

The emergence of the looping-in behavior in nonstoichiometric solutions can be understood by considering the competition between the entropy of counterions and the constraint of electroneutrality. To see this, we examine the low-salt regime and focus on the variation of the polymer concentration in the coacervate. In stoichiometric solutions, the polymer concentration decreases when salt is added, whereas in nonstoichiometric solutions exhibiting the looping-in behavior, it increases. We show here that the dependence of this limiting behavior on the mixing ratio is derived from the standard phase coexistence condition.

The full coexistence condition for solutions containing four ionic components involves 10 unknowns to be solved numerically: eight compositions, the volume ratio of the coacervate, and the Galvani potential (*41*, *42*) between the two phases that is required to enforce

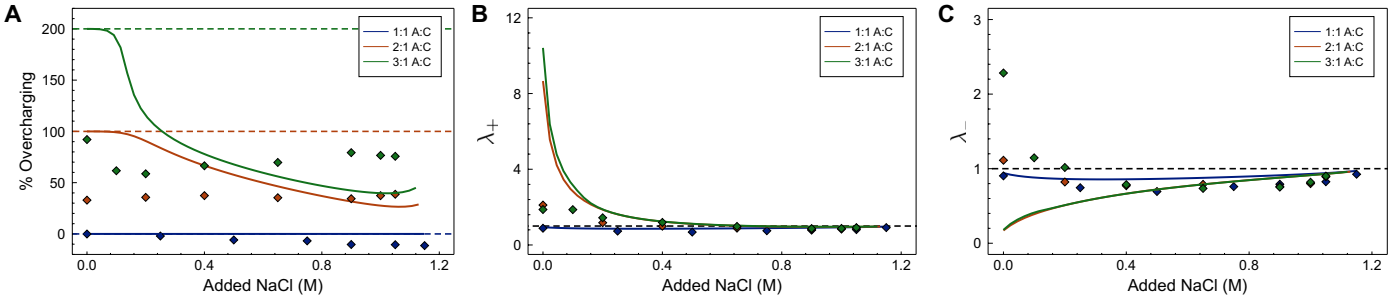

Fig. 6. Comparison of partitioning between theory and experiment. Comparison of overcharging and ion partitioning between theory and experiment. Theoretical predictions are solid lines, and experimental data points are diamond markers. (**A**) Overcharging percentage of the coacervate. (**B**) Ion partition coefficient for cations. (**C**) Ion partition coefficient for anions.

charge neutrality (see Supplementary Text). In the low-salt limit, however, our theoretical results in Fig. 5 suggest that, regardless of the mixing ratio, the polymers are essentially depleted in the supernatant, and they maintain the initial stoichiometric ratio in the coacervate. For simplicity, we first assume that the polymers are entirely depleted in the supernatant and then generalize the analysis to more realistic scenarios. The coexisting phases (Fig. 7) are specified by the total polymer concentration in the coacervate ϕ_2, the total salt concentrations in the supernatant ψ_1 and coacervate ψ_2, and the solution asymmetry factor (*41*)

$$r = \frac{\phi_A - \phi_C}{\phi_A + \phi_C} \tag{7}$$

where ϕ_A and ϕ_C are the initial polyanion and polycation concentrations. The asymmetry factor varies from $r = 0$ in symmetric solutions to $r = 1$ in solutions consisting of only polyanions and cations. Electroneutrality in the coacervate is ensured by introducing counterions with concentration $r\sigma\phi_2$, equal to the charge disparity between the polyions, where σ is the charge density of the PEs. This approximate treatment reduces the number of extra variables and becomes increasingly accurate as the charge asymmetry increases.

In the binary limit (Fig. 7A), with no added salts, we have $\psi_1 = \psi_2 = 0$. The only ions present are those required to maintain electroneutrality in the coacervate. Under these conditions, the equilibrium between the supernatant and coacervate can be treated as that between water and a semidilute polymer solution with concentration ϕ_2^*. Electroneutrality of the coacervate mandates that the concentration of counterions is $r\sigma\phi_2^*$. The concentration ϕ_2^* is fixed by equating the osmotic pressure (or chemical potential of the solvent) between the supernatant and coacervate (*47*). Its value varies with the mixing ratio but always remains of order unity (see Supplementary Text).

In the ternary mixture (Fig. 7B), the added salt partitions to the supernatant and coacervate, with concentrations ψ_1 and ψ_2. Two types of salt ions are now present in the coacervate: added salt ions with concentration ψ_2 and "bound" charge-neutralizing counterions with concentration $r\sigma\phi_2$. Phase coexistence requires additionally the equality of chemical potentials of small ions that, for asymptotically small values of ψ_1 and ψ_2, can be written (see Supplementary Text)

$$\ln\left(\frac{\psi_2(\psi_2 + 2r\sigma\phi_2^*)}{\psi_1^2}\right) = -\mu_{S,2}^{el}(\phi_2^*) \sim \mathcal{O}(1) \tag{8}$$

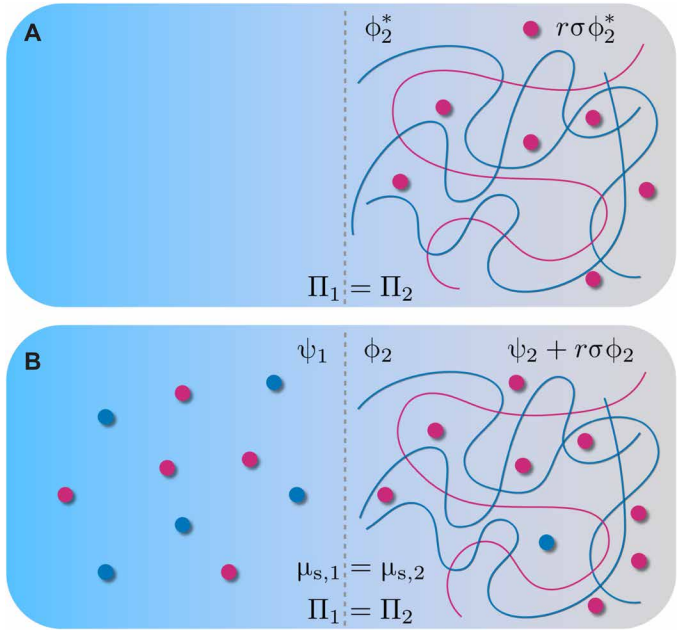

Fig. 7. Schematic representation of the simplified equilibrium conditions at low salt concentrations. (**A**) Binary system with no added salt, where a charge asymmetric coacervate coexists with a pure water supernatant. Equilibrium between the two phases is determined solely by the osmotic pressure balance. (**B**) Ternary system where added salt partitions between the two phases to different extents, and the polymer concentration adjusts in response to this. Equilibrium between the two phases now requires balance of the osmotic pressure and salt ion chemical potentials.

The left-hand side of the equation arises from the mixing entropy of the anions and cations, while the right-hand side contains the excess chemical potential in the coacervate due to electrostatic interactions $\mu_{S,2}^{el}$. The excess chemical potential $\mu_{S,2}^{el}$ is finite and determined by the polymer concentration ϕ_2^*. Balancing Eq. 8 requires that the ratio of salt concentrations on the left-hand side be of order $\mathcal{O}$ (1).

For symmetric solutions with $r = 0$, there are no charge-neutralizing counterions. Their contribution to mixing entropy drops out, and Eq. 8 requires that ψ_2 is comparable to and scales linearly with ψ_1. The ratio ψ_2/ψ_1 defines the limiting slope of the tie-line connecting the supernatant and coacervate phases. Its value is governed by the form of $\mu_{S,2}^{el}$ and depends on factors such as the conformational properties of the PEs (see Supplementary Text).

For asymmetric solutions with $r \approx 1$, the counterion concentration is high, and we have $\psi_2 + 2r\sigma\phi_2^* \approx 2r\sigma\phi_2^*$. Substituting this into Eq. 8 shows that $\psi_2 \sim \psi_1^2 \ll \psi_1$, in sharp contrast to the linear scaling in the symmetric case. The quadratic scaling implies a negative tie-line slope in the low-salt regime. Because the concentration of ions is already high in the coacervate, added salt tends to populate the supernatant phase to maximize the mixing entropy.

The polymer concentration in the coacervate (ϕ_2) then adjusts to restore the osmotic pressure balance upon salt addition. For symmetric solutions ($r = 0$), added salt partitions between the two phases in proportion, with $\psi_2 \sim \psi_1$, which increases the osmotic pressures in both phases. However, the favorable electrostatic interaction between added salt (ψ_2) and polymer in the coacervate (ϕ_2) lowers the osmotic pressure. To make up for this difference, the polymer concentration decreases. For asymmetric solutions ($r \approx 1$), added salt mainly resides in the supernatant ($\psi_2 \ll \psi_1$). To balance the increased osmotic pressure in the supernatant, the coacervate expels water, and the polymer concentration increases. The quantitative details for this behavior are laid out in Supplementary Text.

The looping-in behavior can be rationalized by a crossover from symmetric to asymmetric salt partitioning in weakly asymmetric solutions. For solutions with small yet finite r values, in the low-salt regime, we expect a crossover from symmetric ($\psi_2 \approx \psi_1$) to asymmetric ($\psi_2 \ll \psi_1$) partitioning. Inspecting Eq. 8 shows that this occurs at salt concentrations $2r\sigma\phi_2^* \approx \psi_2 \approx \psi_1$. For counterion concentrations below this threshold, symmetric partitioning dominates, and the polymer concentration decreases; above this threshold, asymmetric partitioning dominates, and the polymer concentration increases with salt addition. This change in slope is responsible for the observed looping-in behavior.

The above analysis assumes that polymers are depleted in the supernatant, and the stoichiometry of the initial solution is maintained in the coacervate, as was suggested by our theoretical predictions (Fig. 5). A competing scenario is the following: The concentrations of polyanions and polycations are equal in the coacervate, irrespective of their initial mixing ratio, and any excess polymer and counterions remain in the supernatant (see Supplementary Text). An analysis of the low-salt coexistence condition under these circumstances reveals a monotonic decrease in polymer concentration with added salt. This scenario resembles more closely the predictions for rod-like chains (fig. S12) and from a previous report (*41*) where the looping-in shape is absent.

The salt partitioning in the low-salt regime for this scenario and for more general composition profiles can still be analyzed by generalizing Eq. 8. If the asymmetry factors for the two coexisting phases are r_1 and r_2, then the counterion concentrations are given by $|r_i|\sigma\phi_i$, where ϕ_i are the total polymer concentrations in each phase. The chemical potential balance equation then reads

$$\ln\left(\frac{\psi_2(\psi_2 + 2|r_2|\sigma\phi_2)}{\psi_1(\psi_1 + 2|r_1|\sigma\phi_1)}\right) = \mu_S^{ex}(\phi_1) - \mu_S^{ex}(\phi_2) \sim \mathcal{O}(1) \qquad (9)$$

Again, the left-hand side comes from the mixing entropy of the small ions, while the right-hand side stems from the excess interactions (e.g., electrostatic correlations) and is of order unity. For asymptotically small values of ψ_1 and ψ_2, the importance of counterions is controlled by the asymmetry factors, and added salt will populate the phase with fewer counterions. This feature underlies the predicted behavior in our theoretical phase diagrams and is unique to nonstoichiometric PE mixtures where charge-neutralizing counterions are prevalent.

However, we emphasize that the response of the polymer concentration in the coacervate depends on the specific form of excess interactions. For instance, we find that electrostatic correlations for flexible chains result in the looping-in shape (Fig. 5 and fig. S12), in accordance with the qualitative picture discussed above, yet alternative treatments of electrostatics do not (*41*). Any excess contributions in addition to electrostatics will complicate this picture further. Nonetheless, Eq. 9 makes it clear that the asymmetry factors r_1 and r_2, alongside the charge neutrality constraint, play an important role in determining the partitioning of ions and underlies the looping-in behavior.

Summary

The looping-in behavior is observed in PECs formed from nonstoichiometric PE mixtures at low salt concentrations. It is characterized by an increase in the coacervate polymer concentration when salt is added, in contrast to what is normally seen in stoichiometric mixtures. The phenomenon, demonstrated in solutions of both synthetic polymers and of polypeptides and DNA over physiologically relevant salinity, is expected to be general.

A dual fluorescent dye-labeling strategy combined with ICP-MS measurements was used to quantify the concentrations of all charged species. This advancement allowed us to prepare phase diagrams unambiguously. The partitioning of polycations, polyanions, and salt ions between the coexisting phases were revealed, which allowed us to quantitatively model the coacervation behavior using a solution thermodynamic model that considers both short-range ion binding and long-range electrostatic interactions. Our theory captured the variation of experimental phase diagrams with the stoichiometric ratio of the oppositely charged PEs and the looping-in behavior at low salt concentrations. A general phase equilibrium consideration showed that the looping-in behavior is attributed to a competition of the mixing entropy of counterions and the electroneutrality constraint in the coacervate. Because excess charge from most PEs must be balanced by counterions, added salt preferentially accumulates in the supernatant to maximize its translational entropy, resulting in a salt-depleted coacervate, which ultimately causes the polymer concentration in the coacervate to increase, to maintain the osmotic pressure balance between the two phases.

Three observations drawn from our study may be generic. First, the concentration asymmetry between oppositely charged polymers in the formed coacervate is reduced compared to the homogeneous mixture (Fig. 3). Second, in strongly asymmetric mixtures, salting-out and salting-in behavior may both be present, resulting in a looping-in or reentrant demixing transition. Third, any molecular factors that cause an abundance of counterions to accumulate in the coacervate phase, such as a severe mismatch in charge density, may cause the looping-in behavior, which may rationalize the effect of pH reported recently (*48*).

Our work directly addresses the effects of compositional heterogeneity on PEC formation, which is ubiquitous in biological PECs. Biological PECs may consist of many types of charged biopolymers, and the impact of asymmetry is likely prominent. A thorough investigation of multiple types of heterogeneity, such as in PE flexibility (*49*), charge density (*48*), or molecular weights, may help to further our understanding of how seemingly nonspecific cellular LLPS regulates biological functions with spatial and temporal precision.

MATERIALS AND METHODS

Synthesis and fluorescent labeling of PEs

Polyacrylamides with pendant ammonium or sulfate groups at identical chain lengths (N = 50) and charge density were synthesized from the same narrow-disperse polymer precursor made by reversible addition-fragmentation transfer (RAFT) polymerization, following our recently reported method (*26*). PGA and PLL were synthesized via NCA polymerization, following previously reported procedures (*50*).

RB was conjugated to positively charged polyacrylamide according to previously reported procedure (*26*). The fraction of dye-labeled polycations was determined to be approximately 1 per 10 polymer chains by ^{1}H NMR spectroscopy. The concentration of polycations was calculated by measuring the absorption at 566 nm for the labeled polycation. Sulfo-Cy5-amine was conjugated to the carboxylate end group from the RAFT agent on negatively charged polyacrylamide via carbodiimide coupling. The fraction of dye-labeled polyanions was determined to be approximately 1 per 87 polymer chains based on the measured absorption and extinction coefficient at 649 nm. Sulfo-Cy5-amine was conjugated to the carboxylate groups on negatively charged PGA via carbodiimide coupling. The fraction of dye-labeled PGA was determined to be approximately 1 per 295 polymer chains based on the measured absorption and extinction coefficient at 649 nm. FITC was conjugated to the amine groups on negatively charged PLL. The fraction of dye-labeled PLL was determined to be approximately 1 per 32 polymer chains based on the measured absorption and extinction coefficient at 494 nm.

Mixing of oppositely charged PEs at various stoichiometries had a negligible effect on the extinction coefficients of the labeled dyes (fig. S2), making the dual-fluorescent labeling a convenient means to independently and accurately quantify oppositely charged PE concentrations in different phases.

Measurement of experimental phase diagrams

Solutions of anionic and cationic PEs were mixed at an overall polymer concentration of 100 mM with varying added NaCl concentrations from 0 to 1.2 M. For charged polyacrylamides, the pH value of stock solutions was adjusted to 4.2 using 1 M HCl, while for charged polypeptides, the pH value of stock solutions was adjusted to 7.4 using 1 M NaOH. The ion content in the solutions included a baseline of 100 mM of Na^+ and Cl^- counterions from the PEs (split between cations and anions, depending on the mixing ratio), as well as any additional ions from the added salt. Mixtures were further equilibrated at room temperature for another 2 days before measurement of polymer concentrations. The volume of each phase in the phase-separated mixtures was measured by a calibrated pipet. The solution phase was diluted before the measurement of polymer concentration using the calibration curve of labeled fluorophore. The coacervate phase was lyophilized and redissolved in 1 ml of NaCl solution (2 M) before further dilution for measurement. Polymer concentrations in the solution phase and coacervate phase were quantified using the calibration curve. Three independent experimental replicates were performed for all data points to construct the phase diagrams.

For the PECs formed from polyacrylamides, Na^+ and Cl^- concentrations were measured using ICP-MS. A standard calibration curve was first generated by measuring NaCl solution at different concentrations. All measurements were performed by diluting a measured small aliquot of the coacervate or supernatant to deionized water containing 0.5 mM KOH, which was used to prevent phase separation during dilution by deprotonation of polycations in the mixture. The solution phase was directly diluted for measurement. The coacervate phase was first lyophilized and redissolved in 200 μl of KBr solution (1 M) before further dilution. Three independent experimental replicates were performed for all data points to construct the phase diagrams.

Calculation of theoretical phase diagrams

Theoretical phase diagrams were constructed in a manner that resembles the experimental mixing protocol. The initial solution compositions were specified at a total polymer concentration of 100 mM, split between polyanions and polycations based on the stoichiometric mixing ratio. A baseline concentration of counterions was also added to match the PE charge and maintain electroneutrality in the bulk solution. For any initial solution composition, the supernatant and coacervate concentrations were determined by balancing the chemical potential of each component between the phases (see Supplementary Text for more details). Full coexistence diagrams were obtained by screening the amount of added salt and calculating the coexistence condition at each point until reaching the upper maximum ion concentration at which phase separation ceased to occur. Because of the fixed, initial polymer concentration, this upper point on the binodal diagram was found to fall off-center from the true maximum ion concentration within the two-phase region, as indicated by the clipping of the binodal curves at high salt concentrations in Fig. 5.

To match the theoretical predictions with the experimental phase diagrams, the model parameters were determined as follows: The structural parameters for the PEs and salt ions were estimated from experimental data. The monomeric volumes and the chain lengths were calculated in reference to a reference volume $v_0 = 0.03$ nm^3, i.e., the volume of water molecule. On the basis of this reference, we set the polyanion and polycation chain lengths at $N_A = N_C = 50$, the monomeric volumes at $\omega_A = \omega_C = 10$, and the ion volumes at $\omega_+ = \omega_- = 3$. The large ion volumes could be envisioned to represent the solvation shell sizes in aqueous solutions (*38*). Last, the statistical segment lengths of the chains were set to $b_A = 0.75\,\omega_A^{1/3}$ and $b_C = 0.75\,\omega_C^{1/3}$, comparable to the monomeric diameter. The Flory-Huggins parameter between polymer and solvent was held at $\chi_{PW} = 0.5$, which is expected for polymers in θ solvent. The binding free energies were tuned so that the theory matches the maximum salt concentration for the 1:1 mixture, giving $\Delta G_{A+} = \Delta G_{C-} = -1.0 k_B T$ and $\Delta G_{AC} = -1.55 k_B T$, consistent with the range of values reported in literature (*51*, *52*). These values were then used to calculate the full phase diagram for the 1:1 A:C mixture and to predict the phase diagrams for the 2:1 and 3:1 A:C mixtures.

SUPPLEMENTARY MATERIALS

Supplementary material for this article is available at http://advances.sciencemag.org/cgi/content/full/7/31/eabg8654/DC1

REFERENCES AND NOTES

1. H. G. Bungenberg de Jong, H. R. Kruyt, Coacervation (partial miscibility in colloid systems). *Proc. Royal Acad. Amsterdam* **32**, 849–856 (1929).
2. Q. Wang, J. B. Schlenoff, The polyelectrolyte complex/coacervate continuum. *Macromolecules* **47**, 3108–3116 (2014).
3. B. Panganiban, B. Qiao, T. Jiang, C. DelRe, M. M. Obadia, T. D. Nguyen, A. A. A. Smith, A. Hall, I. Sit, M. G. Crosby, P. B. Dennis, E. Drockenmuller, M. O. de la Cruz, T. Xu, Random

heteropolymers preserve protein function in foreign environments. *Science* **359**, 1239–1243 (2018).
4. A. Akinc, D. M. Lynn, D. G. Anderson, R. Langer, Parallel synthesis and biophysical characterization of a degradable polymer library for gene delivery. *J. Am. Chem. Soc.* **125**, 5316–5323 (2003).
5. Y. Liu, T. M. Reineke, Hydroxyl stereochemistry and amine number within poly(glycoamidoamine)s affect intracellular DNA delivery. *J. Am. Chem. Soc.* **127**, 3004–3015 (2005).
6. D. S. Hwang, J. H. Waite, M. Tirrell, Promotion of osteoblast proliferation on complex coacervation-based hyaluronic acid – Recombinant mussel adhesive protein coatings on titanium. *Biomaterials* **31**, 1080–1084 (2010).
7. S. Lim, Y. S. Choi, D. G. Kang, Y. H. Song, H. J. Cha, The adhesive properties of coacervated recombinant hybrid mussel adhesive proteins. *Biomaterials* **31**, 3715–3722 (2010).
8. C. J. Decker, R. Parker, P-bodies and stress granules: Possible roles in the control of translation and mRNA degradation. *Cold Spring Harb. Perspect. Biol.* **4**, a012286 (2012).
9. P. Anderson, N. Kedersha, Stress granules: The tao of RNA triage. *Trends Biochem. Sci.* **33**, 141–150 (2008).
10. C. P. Brangwynne, C. R. Eckmann, D. S. Courson, A. Rybarska, C. Hoege, J. Gharakhani, F. Julicher, A. A. Hyman, Germline p granules are liquid droplets that localize by controlled dissolution/condensation. *Science* **324**, 1729–1732 (2009).
11. E. Sokolova, E. Spruijt, M. M. K. Hansen, E. Dubuc, J. Groen, V. Chokkalingam, A. Piruska, H. A. Heus, W. T. S. Huck, Enhanced transcription rates in membrane-free protocells formed by coacervation of cell lysate. *Proc. Natl. Acad. Sci. U.S.A.* **110**, 11692–11697 (2013).
12. M. Du, Z. J. Chen, DNA-induced liquid phase condensation of cGAS activates innate immune signaling. *Science* **361**, 704–709 (2018).
13. J. Berry, S. C. Weber, N. Vaidya, M. Haataja, C. P. Brangwynne, RNA transcription modulates phase transition-driven nuclear body assembly. *Proc. Natl. Acad. Sci. U.S.A.* **112**, E5237–E5245 (2015).
14. J. E. Lee, P. I. Cathey, H. Wu, R. Parker, G. K. Voeltz, Endoplasmic reticulum contact sites regulate the dynamics of membraneless organelles. *Science* **367**, eaay7108 (2020).
15. S. Markmiller, S. Soltanieh, K. L. Server, R. Mak, W. Jin, M. Y. Fang, E.-C. Luo, F. Krach, D. Yang, A. Sen, A. Fulzele, J. M. Wozniak, D. J. Gonzalez, M. W. Kankel, F.-B. Gao, E. J. Bennett, E. Lécuyer, G. W. Yeo, Context-dependent and disease-specific diversity in protein interactions within stress granules. *Cell* **172**, 590–604.e13 (2018).
16. E. M. Courchaine, A. Lu, K. M. Neugebauer, Droplet organelles? *EMBO J.* **35**, 1603–1612 (2016).
17. Y. Shin, C. P. Brangwynne, Liquid phase condensation in cell physiology and disease. *Science* **357**, eaaf4382 (2017).
18. S. L. Perry, Phase separation: Bridging polymer physics and biology. *Curr. Opin. Colloid Interface Sci.* **39**, 86–97 (2019).
19. J. Pelta, F. Livolant, J. L. Sikorav, DNA aggregation induced by polyamines and cobalthexamine. *J. Biol. Chem.* **271**, 5656–5662 (1996).
20. E. Raspaud, M. O. de la Cruz, J.-L. Sikorav, F. Livolant, Precipitation of DNA by polyamines: A polyelectrolyte behavior. *Biophys. J.* **74**, 381–393 (1998).
21. H. Zhang, S. Elbaum-Garfinkle, E. M. Langdon, N. Taylor, P. Occhipinti, A. A. Bridges, C. P. Brangwynne, A. S. Gladfelter, RNA controls PolyQ protein phase transitions. *Mol. Cell* **60**, 220–230 (2015).
22. M. Feric, N. Vaidya, T. S. Harmon, D. M. Mitrea, L. Zhu, T. M. Richardson, R. W. Kriwacki, R. V. Pappu, C. P. Brangwynne, Coexisting liquid phases underlie nucleolar subcompartments. *Cell* **165**, 1686–1697 (2016).
23. E. Spruijt, A. H. Westphal, J. W. Borst, M. A. C. Stuart, J. van der Gucht, Binodal compositions of polyelectrolyte complexes. *Macromolecules* **43**, 6476–6484 (2010).
24. L. Li, S. Srivastava, M. Andreev, A. B. Marciel, J. J. de Pablo, M. V. Tirrell, Phase behavior and salt partitioning in polyelectrolyte complex coacervates. *Macromolecules* **51**, 2988–2995 (2018).
25. L.-W. Chang, T. K. Lytle, M. Radhakrishna, J. J. Madinya, J. Vélez, C. E. Sing, S. L. Perry, Sequence and entropy-based control of complex coacervates. *Nat. Commun.* **8**, 1273 (2017).
26. J. Lou, S. Friedowitz, J. Qin, Y. Xia, Tunable coacervation of well-defined homologous polyanions and polycations by local polarity. *ACS Cent. Sci.* **5**, 549–557 (2019).
27. S. Srivastava, M. V. Tirrell, Polyelectrolyte complexation, in *Advances in Chemical Physics* (John Wiley & Sons Inc., 2016), pp. 499–544.
28. C. E. Sing, S. L. Perry, Recent progress in the science of complex coacervation. *Soft Matter* **16**, 2885–2914 (2020).
29. A. M. Rumyantsev, N. E. Jackson, J. J. de Pablo, Polyelectrolyte complex coacervates: Recent developments and new frontiers. *Annu. Rev. Condens. Matter Phys.* **12**, 155–176 (2021).
30. J. T. G. Overbeek, M. J. Voorn, Phase separation in polyelectrolyte solutions. Theory of complex coacervation. *J. Cell. Physiol.* **49**, 7–26 (1957).
31. V. Y. Borue, I. Y. Erukhimovich, A statistical theory of weakly charged polyelectrolytes: Fluctuations, equation of state and microphase separation. *Macromolecules* **21**, 3240–3249 (1988).
32. J. Qin, J. J. de Pablo, Criticality and connectivity in macromolecular charge complexation. *Macromolecules* **49**, 8789–8800 (2016).
33. M. O. de la Cruz, L. Belloni, M. Delsanti, J. P. Dalbiez, O. Spalla, M. Drifford, Precipitation of highly charged polyelectrolyte solutions in the presence of multivalent salts. *J. Chem. Phys.* **103**, 5781–5791 (1995).
34. M. Muthukumar, Theory of counter-ion condensation on flexible polyelectrolytes: Adsorption mechanism. *J. Chem. Phys.* **120**, 9343–9350 (2004).
35. A. Salehi, R. G. Larson, A molecular thermodynamic model of complexation in mixtures of oppositely charged polyelectrolytes with explicit account of charge association/dissociation. *Macromolecules* **49**, 9706–9719 (2016).
36. T. K. Lytle, C. E. Sing, Transfer matrix theory of polymer complex coacervation. *Soft Matter* **13**, 7001–7012 (2017).
37. S. Friedowitz, A. Salehi, R. G. Larson, J. Qin, Role of electrostatic correlations in polyelectrolyte charge association. *J. Chem. Phys.* **149**, 163335 (2018).
38. M. Ghasemi, S. Friedowitz, R. G. Larson, Analysis of partitioning of salt through doping of polyelectrolyte complex coacervates. *Macromolecules* **53**, 6928–6945 (2020).
39. S. Adhikari, M. A. Leaf, M. Muthukumar, Polyelectrolyte complex coacervation by electrostatic dipolar interactions. *J. Chem. Phys.* **149**, 163308 (2018).
40. A. M. Rumyantsev, N. E. Jackson, B. Yu, J. M. Ting, W. Chen, M. V. Tirrell, J. J. de Pablo, Controlling complex coacervation via random polyelectrolyte sequences. *ACS Macro Lett.* **8**, 1296–1302 (2019).
41. P. Zhang, N. M. Alsaifi, J. Wu, Z.-G. Wang, Polyelectrolyte complex coacervation: Effects of concentration asymmetry. *J. Chem. Phys.* **149**, 163303 (2018).
42. P. Zhang, N. M. Alsaifi, J. Wu, Z.-G. Wang, Salting-out and salting-in of polyelectrolyte solutions: A liquid-state theory study. *Macromolecules* **49**, 9720–9730 (2016).
43. S. L. Perry, Y. Li, D. Priftis, L. Leon, M. Tirrell, The effect of salt on the complex coacervation of vinyl polyelectrolytes. *Polymers* **6**, 1756–1772 (2014).
44. M. Radhakrishna, K. Basu, Y. Liu, R. Shamsi, S. L. Perry, C. E. Sing, Molecular connectivity and correlation effects on polymer coacervation. *Macromolecules* **50**, 3030–3037 (2017).
45. K. T. Delaney, G. H. Fredrickson, Theory of polyelectrolyte complexation—Complex coacervates are self-coacervates. *J. Chem. Phys.* **146**, 224902 (2017).
46. K. Shen, Z.-G. Wang, Polyelectrolyte chain structure and solution phase behavior. *Macromolecules* **51**, 1706–1717 (2018).
47. A. M. Rumyantsev, E. B. Zhulina, O. V. Borisov, Complex coacervate of weakly charged polyelectrolytes: Diagram of states. *Macromolecules* **51**, 3788–3801 (2018).
48. L. Li, S. Srivastava, S. Meng, J. M. Ting, M. V. Tirrell, Effects of non-electrostatic intermolecular interactions on the phase behavior of pH-sensitive polyelectrolyte complexes. *Macromolecules* **53**, 7835–7844 (2020).
49. A. Shakya, M. Girard, J. T. King, M. O. de la Cruz, Role of chain flexibility in asymmetric polyelectrolyte complexation in salt solutions. *Macromolecules* **53**, 1258–1269 (2020).
50. H. Lu, J. Cheng, Hexamethyldisilazane-mediated controlled polymerization of α-amino acid *N*-carboxyanhydrides. *J. Am. Chem. Soc.* **129**, 14114–14115 (2007).
51. J. Fu, H. M. Fares, J. B. Schlenoff, Ion-pairing strength in polyelectrolyte complexes. *Macromolecules* **50**, 1066–1074 (2017).
52. J. B. Schlenoff, M. Yang, Z. A. Digby, Q. Wang, Ion content of polyelectrolyte complex coacervates and the donnan equilibrium. *Macromolecules* **52**, 9149–9159 (2019).
53. J. R. Vieregg, M. Lueckheide, A. B. Marciel, L. Leon, A. J. Bologna, J. R. Rivera, M. V. Tirrell, Oligonucleotide–peptide complexes: Phase control by hybridization. *J. Am. Chem. Soc.* **140**, 1632–1638 (2018).
54. O. T. du Boullay, N. Saffon, J.-P. Diehl, B. Martin-Vaca, D. Bourissou, Organo-catalyzed ring opening polymerization of a 1, 4-dioxane-2, 5-dione deriving from glutamic acid. *Biomacromolecules* **11**, 1921–1929 (2010).
55. A. N. Semenov, M. Rubinstein, Thermoreversible gelation in solutions of associative polymers. 1. Statics. *Macromolecules* **31**, 1373–1385 (1998).
56. A. Kundagrami, M. Muthukumar, Theory of competitive counterion adsorption on flexible polyelectrolytes: Divalent salts. *J. Chem. Phys.* **128**, 244901 (2008).
57. Z.-G. Wang, Fluctuation in electrolyte solutions: The self energy. *Phys. Rev. E* **81**, 021501 (2010).
58. M. C. Villet, G. H. Fredrickson, Efficient field-theoretic simulation of polymer solutions. *J. Chem. Phys.* **141**, 224115 (2014).
59. K. T. Delaney, G. H. Fredrickson, Recent developments in fully fluctuating field-theoretic simulations of polymer melts and solutions. *J. Phys. Chem. B* **120**, 7615–7634 (2016).

Acknowledgments

Funding: This research has been supported by the National Science Foundation CAREER Award through DMR-1846547. Y.X. thanks the Sloan Foundation for a Sloan Research Fellowship. J.Q. acknowledges support from the 3M Nontenured Faculty Award and the Hellman Scholar Award. This work is supported by the startup funds from the Department of Chemical Engineering and the Department of Chemistry at the Stanford University.

Author contributions: J.L., K.P.B., and Y.X. designed experimental research. S.F. and J.Q. designed theoretical models and analysis. J.L., K.P.B., and K.W. performed experimental synthesis and characterization. S.F. performed theoretical modeling and analysis. S.F., J.L., K.P.B., Y.X., and J.Q. wrote the manuscript. **Competing interests:** The authors declare that they have no competing interests. **Data and materials availability:** All data needed to evaluate the conclusions in the paper are present in the paper and/or the Supplementary Materials. Additional data related to this paper may be requested from the authors.

Submitted 1 February 2021
Accepted 15 June 2021
Published 30 July 2021
10.1126/sciadv.abg8654

Citation: S. Friedowitz, J. Lou, K. P. Barker, K. Will, Y. Xia, J. Qin, Looping-in complexation and ion partitioning in nonstoichiometric polyelectrolyte mixtures. *Sci. Adv.* **7**, eabg8654 (2021).